Catalytic low-temperature combustion of dichloromethane over V–Ni/TiO$_2$ catalyst

Xinhua Zhang,[a] Zhiying Pei,[a] Xingjie Ning,[a] Hanfeng Lu[b] and Haifeng Huang*[a]

Vanadium–nickel mixed oxides supported on TiO$_2$ (anatase) were prepared by wet impregnation using ammonium metavanadate and nickel nitrate aqueous solution. The performance of as-prepared samples in catalytic dichloromethane (DCM) combustion was investigated, and their physicochemical properties were characterized in detail by X-ray diffraction, N$_2$ physisorption, H$_2$ temperature-programmed reduction, NH$_3$ temperature-programmed desorption, and Raman spectroscopy analyses. Results showed DCM combustion activity over V–Ni/TiO$_2$ catalyst was superior to that of V$_2$O$_5$/TiO$_2$ and NiO/TiO$_2$ catalysts. DCM could be completely converted into CO$_2$, HCl, and a little amount of CO over Ni–V/TiO$_2$ catalyst at 350 °C, the toxic by-products, such as CH$_3$Cl, aldehydes and phosgene could not be observed by online IR spectroscopy. The high catalytic activity, selectivity, and stability of V–Ni/TiO$_2$ catalyst could be due to the good oxidative dehydrogenation ability (ODH), the good reducibility of active oxygen species, and suitable strength of Lewis acidic sites upon introduction of nickel oxide.

1. Introduction

Chlorinated volatile organic compounds (CVOCs) such as dichloromethane (DCM) and trichloroethylene (TCE) are commercially produced and used for many purposes in different industries. Almost all CVOCs emitted are hazardous to the environment and public health; thus, stricter emission ceilings for each country are set. Catalytic abatement of CVOCs is an efficient, cost-effective, and environmentally sound way to abate these harmful emissions because of low energy consumption, high efficiency, and selectivity.[1,2] Catalyst is undoubtedly a key factor to implement this technique. Generally, most reported catalysts for CVOC combustion are supported noble metals,[1–3] transition metal oxides,[4–9] and zeolites.[10–12]

The ultimate aim of CVOCs catalytic combustion is to completely transform these hazardous materials into environmentally harmless compounds, such as H$_2$O, CO$_2$, and HCl. However, almost all catalysts are influenced by chlorine species produced by CVOCs decomposition. The interaction of catalysts with chlorine species usually leads to the catalyst's partial or complete deactivation, which further results in crystallite growth (sintering and agglomeration), carbon deposition, change in physical properties, poisoning by chlorine species, and leaching out of active phase.[6,7,13] The catalyst applied in CVOCs destruction should be not only highly active and

selective at relatively low temperature, but also maintain high resistance to chlorine and its derivatives.[14,15]

Vanadium-containing catalysts are always shown to have good stability in Cl$_2$–HCl atmosphere. Especially, vanadia supported on TiO$_2$ are reportedly superior to the other conventional carriers such as Al$_2$O$_3$ and SiO$_2$ in several redox reactions because of the strong metal-support interactions (SMSI),[16] which could improve the activity of surface oxygen on the catalyst. Even more interesting is the performance of V$_2$O$_5$/TiO$_2$ catalyst, which can be significantly changed by doping some other metal oxides as impurities or promoters.[17,18]

Monochloromethane (MCM) is usually a main by-product derived from the interaction of methoxy species and HCl in DCM combustion.[2,19] MCM is more recalcitrant than DCM because of its low electrophilicity in central carbon atom. Thus, the transformation of MCM is more difficult than that of DCM.[20] Nickel-supported catalyst usually shows good oxidative dehydrogenation and hydrodehalogenation ability in many redox reactions.[21,22] In the present work, a catalyst with vanadium–nickel mixed oxides supported on TiO$_2$ was prepared and used for DCM combustion; our aim is to investigate the selectivity, activity and stability of the catalyst in DCM combustion at a relatively low temperature range. To the best of our knowledge, this catalyst has not yet been reported for use in DCM combustion.

[a]College of Biological and Environmental technology, Zhe Jiang University of Technology, Hang Zhou 310032, PR China. E-mail: hhf66@zjut.edu.cn; Tel: +86-571-88320385

[b]College of Chemical Engineering, Zhe Jiang University of Technology, Hang Zhou 310032, PR China

2. Experimental

2.1 Catalyst preparation

The catalyst with vanadium–nickel mixed oxides supported on TiO$_2$ was prepared by conventional impregnation method. In a

typical procedure, a certain amount of precursors NH_4VO_3 (Shanghai SSS Reagent Co., Ltd), $Ni(NO_3)_2 \cdot 6H_2O$ (Shanghai Qingong Inorganic Co., Ltd), and oxalic acid were dissolved in deionized water under magnetic stirring at 60 °C. Then, 2.0 g of TiO_2 support (Nanjing Haitai Nano materials Co., Ltd) was added to the solution under vigorous stirring for 20 min. After dehydrating the slurry in a rotary evaporator in a 70 °C water bath, the residues were dried at 110 °C for 12 h, and finally calcined in air at 500 °C for 5 h in a muffle furnace. The nominal loaded active phase of the as-prepared catalyst was 3% weight of vanadium atoms and 7% weight of nickel atoms, respectively, corresponding to the monolayer/sub-monolayer of mixed oxides on TiO_2 support,[16,23] and the as-prepared catalyst was denoted as V–Ni/TiO_2 hereafter. For comparison, NiO/TiO_2 and V_2O_5/TiO_2 catalysts loaded with 10% weight of nickel atoms and 10% weight of vanadium atoms, respectively, were prepared in the same way as aforementioned.

2.2 Catalyst characterization

Powder X-ray diffraction (XRD) patterns of the samples were recorded on an X'Pert Pro powder diffractometer using Cu Ka ($\lambda = 0.154056$ nm) radiation (40 kV and 30 mA). The diffractograms were recorded within $2\theta = 10°–80°$ with a step size of 0.02° and a step time of 10 s. Crystal sizes were calculated using the Scherrer equation: $d = \dfrac{0.9\lambda}{B\cos\theta}$, where d is the crystal particle diameter (Å), λ is the wavelength (Å), B is the broadening of diffraction line measured at half its maximum intensity (radians), and θ is the reflection angle (radians). The nitrogen adsorption and desorption isotherms were measured at −196 °C on a Micromeritics ASAP 2010 in a static mode. All samples were outgassed at 250 °C for 3 h before measurement. The specific surface area was calculated using the BET model. H_2 temperature-programmed reduction (H_2-TPR) was investigated on FINE SORB-3010 E instrument by heating 200 mg of samples in a H_2 (10 vol%)/Ar flow (30 mL min^{-1}) at a heating rate of 10 °C min^{-1} from 50 to 900 °C. All samples were heated in a highly pure Ar flow at 200 °C for 1 h and then cooled to 50 °C before measurement. NH_3 temperature-programmed desorption (NH_3-TPD) was performed on FINE SORB-3010 E instrument equipped with a TCD. Prior to ammonia adsorption, the samples (100 mg) were pretreated in a highly pure He stream (35 mL min^{-1}) at 500 °C for 1 h. After cooling down to 50 °C, the samples were exposed to a flow of 20 vol% NH_3/He mixture (30 mL min^{-1}) for 1 h and subjected to a He flow for another 1 h to remove physically bounded ammonia. Finally, a desorption performance was examined in a He flow (30 mL min^{-1}) from 50 °C to 500 °C at a heating rate of 10 °C min^{-1}. Raman spectra were obtained on a Raman spectrometer (HR 800 Lab Ram, Horiba Jobin Yvon, Villeneuve d'Ascq, France) equipped with a 531.95 nm Ar$^+$ ion laser (frequency-doubled Nd: YAG, 20 mW) and a CCD detector (multichannel, air cooled). The sample cell was purged with a He stream for 30 min before pyridine adsorption, and then 100 μL pyridine was injected. The sample was exposed to the pyridine vapor at ambient temperature for 30 min, and then purged with

He for another 30 min to remove the physisorbed pyridine before measurement. The carbon deposit of the aged V–Ni/TiO_2 after the stability test was investigated in TEM (Philips-FEI, Tecnai G2 F30 S-Twin). The sample was dispersed in absolute alcohol, and then supported on a copper grid before observation.

2.3 Catalytic activity test

Catalytic experiments were performed in a fixed bed tubular reactor (quartz glass; 10 mm i.d.) at an ambient pressure. 0.2 g of catalyst was placed in the middle of the reactor and diluted with 0.8 g of quartz sand. Both ends of catalyst bed were packed with quartz wool to prevent the catalyst from draining off. A DCM feed gas was generated by bubbling the air (20.8% O_2 and 79.2% N_2) at a suitable flow rate through a saturator in ice bath, and a bypass flow of air was used to balance the total flow rate that gave the desired gas hourly space velocity (GHSV) in the catalyst bed. The feed DCM concentration was kept constant at 1000 ppm with a corresponding GHSV of 15 000 mL g^{-1} h^{-1} in all experiments. All gas flow was controlled with mass flow controllers (Beijing Seven-star Electronics Co., Ltd). The effluent gases were analyzed online with an FT-IR spectrometer (Vertex 70; scan rate = 32 scans s^{-1}; resolution = 2.5 cm^{-1}) and a GC-9790 gas chromatograph equipped with FID and TCD. A Proapak Q column was used to separate CO_2 and organic compounds, whereas CO separation was achieved using a 5 A molecular sieve column. The concentration of Cl_2 and HCl were analyzed by bubbling the effluent through a 0.0125 N NaOH solution, a further detailed analytic process was described elsewhere.[24]

3. Results and discussions

3.1 Catalytic activity results

Fig. 1 shows that a complete DCM conversion was achieved between 350 and 450 °C for all investigated samples. The V–Ni/TiO_2 bi-component sample showed better performance than the mono-component ones and completely converted DCM at a lower temperature. The T_{90} value (temperatures with 90% DCM
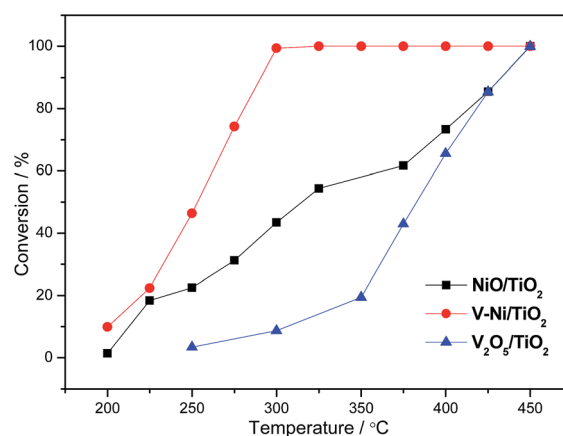

Fig. 1 Light-off curves of DCM over as-prepared catalysts. Gas composition: 1000 ppm DCM in air, GHSV = 15 000 mL g^{-1} h^{-1}.

conversion achieved) of V–Ni/TiO$_2$ was only 290 °C, about 140 °C lower than that of NiO/TiO$_2$ and V$_2$O$_5$/TiO$_2$ samples (T_{90} were about 433 °C), which was superior to that of some noble metal catalysts in the same conditions.[1,2]

A high conversion at a low temperature is not the only criterion in identifying a good DCM combustion catalyst; the product selectivity is also very important because a poor selectivity may result in more toxic and recalcitrant by-products than the original reactant. Thus, the product selectivity of V–Ni/TiO$_2$ catalyst for DCM combustion was investigated through online IR spectroscopy analysis at different temperatures.

Fig. 2 shows an absorption band at 2360 cm^{-1} with a shoulder at 2343 cm^{-1} is attributed to the asymmetric stretching vibration of CO$_2$; meanwhile, the band at 680 cm^{-1} is ascribed to the deformation vibration of CO$_2$. Doublet at 2173 and 2116 cm^{-1} are usually attributed to the stretching vibration CO. The weak thin bands at 3100–2700 cm^{-1} indicate the presence of HCl in the gas phase.[1] Moreover, a band located at 763 cm^{-1} is the stretching vibration of C–Cl bond, also the bands at 1276 and 1260 cm^{-1} are attributed to the twisting vibration and wagging vibrations of methylene group in the DCM molecule, respectively. Indeed, as informed from Fig. 2, the intensity of absorption bands of CO$_2$ and HCl significantly increased as compared with that of CO with the reaction temperature, while the intensity of absorption bands corresponding to DCM gradually decreased and completely disappeared at 350 °C. It should be mentioned that the bands located at 1750–1700 cm^{-1}, which are corresponding to the stretching vibration of C=O in organic molecules, cannot be observed in Fig. 2, indicating no aldehydes and phosgene were formed, or their concentrations were too low to be detected, although these compounds are usually found as intermediates in CVOCs combustion.

Fig. 3 showed DCM conversion and products distribution over the investigated samples. The conversion of DCM over V$_2$O$_5$/TiO$_2$ and V–Ni/TiO$_2$ samples underwent a likely adaptive period at a low temperature range (below 300 and 225 °C, respectively), then, the conversion sped up with the reaction temperature further increased, which is much different from a
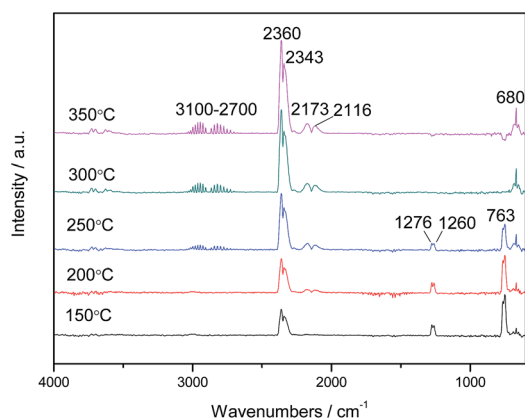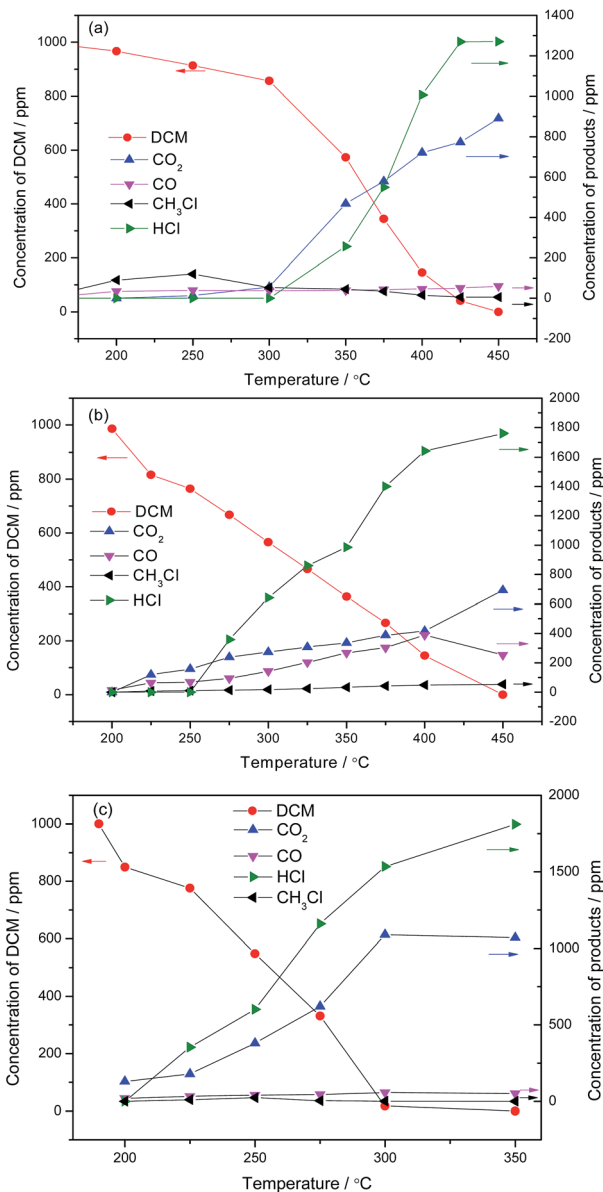

Fig. 3 DCM conversion and the products distribution: (a) V$_2$O$_5$/TiO$_2$; (b) NiO/TiO$_2$; (c) V–Ni/TiO$_2$. Gas composition: 1000 ppm DCM in air, GHSV = 15 000 mL g^{-1} h^{-1}.

quasi-steady conversion of DCM over NiO/TiO$_2$ catalyst. The main products of all investigated samples were CO$_2$, CO, HCl, and CH$_3$Cl. However, their distributions were far from identical, depending on the used catalysts. Using V$_2$O$_5$/TiO$_2$, DCM conversion yielded a larger amount of CH$_3$Cl compared with Ni contained catalysts at low temperatures (below 300 °C). However, the yield of CH$_3$Cl obviously decreased and the selectivity of CO and HCl significantly increased with DCM conversion using NiO/TiO$_2$ catalyst. Using V–Ni/TiO$_2$, the main products of DCM conversion were CO$_2$ and HCl, and their selectivities were exceeded 95% and 90%, respectively, at 350 °C. A little amount of CO was also detected when DCM conversion was performed on V–Ni/TiO$_2$ catalyst, and the yield of CO increased from 20 ppm to 51 ppm with the temperature

Fig. 2 On-line IR spectra of DCM conversion over V–Ni/TiO$_2$ catalyst with the increased reaction temperature.

elevated from 200 °C to 350 °C, and the results are consistent with that of IR spectra.

3.2 Characterization results of catalysts

3.2.1 XRD results. The XRD patterns of as-prepared samples are shown in Fig. 4; corresponding crystallite sizes are listed in Table 1. It is informed from Fig. 4 that the characteristic diffraction peaks of tetragonal anatase TiO_2 (PDF 65-5714) appeared on all investigated samples,[25] also the feature diffractions of NiO (PDF 65-2901) appeared on NiO/TiO_2 and $V–Ni/TiO_2$ samples with different intensities. For V_2O_5/TiO_2 sample, the characteristic peaks of V_2O_5 (PDF 41-1426) can be observed, suggesting the formation of a bulk V_2O_5 on the surface of TiO_2. However, there are no reflections of the crystalline V_2O_5 presented on $V–Ni/TiO_2$ sample, indicating a relatively homogeneous dispersion of V_2O_5 on the catalyst, or the particles are too small to be identified by the conventional X-ray diffraction method. As shown in Table 1, the crystalline size of $V–Ni/TiO_2$ sample is much smaller than that of V_2O_5/TiO_2, suggesting the introduction of nickel oxides decrease the average crystalline sizes of TiO_2 NPs, by providing dissimilar boundaries and suppressing the mass transportation, similar results are also reported by Li *et al.*[26] The result is consistent with that of N_2 physisorption, as the specific surface area of $V–Ni/TiO_2$ was also increased with nickel oxide introduced.

3.2.2 H_2-TPR results. H_2-TPR experiments were performed to investigate the reducibility of as-prepared catalysts. As presented in Fig. 5, TPR of NiO/TiO_2 mainly exhibits two partially
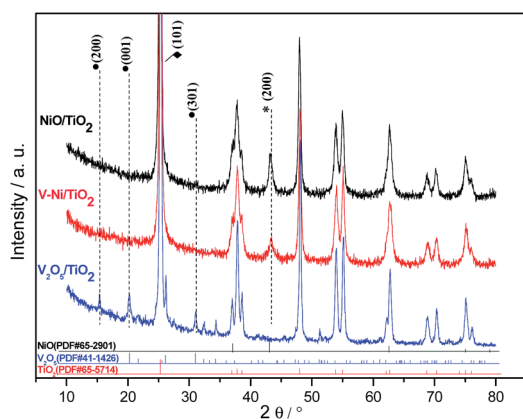
Fig. 4 XRD patterns of as-prepared catalysts. (◆: TiO_2; *:NiO; ●: V_2O_5).

Table 1 Textural properties of the investigated samples

Samples	Crystallite size[a]/nm	BET area/m^2 g^{-1}	T_{90}/°C
TiO_2	23.2	56.72	—
NiO/TiO_2	22.0	66.08	433
$V–Ni/TiO_2$	21.8	71.94	290
V_2O_5/TiO_2	33.5	27.01	433

[a] The value estimated by Scherrer equation, applied to the (1 0 1) reflection of TiO_2.
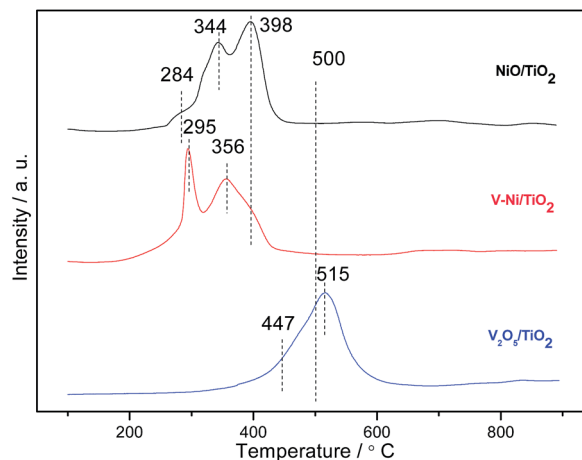
Fig. 5 H_2-TPR profiles of as-prepared catalysts.

overlapped reduction peaks below 400 °C and a broad feature between 500 °C and 800 °C or higher. Since Ni^{2+} species are usually reduced to Ni^0 without formation of intermediates, thus, the reduction peaks in NiO/TiO_2 sample could be assigned to the reduction of different nickel species. The peak located in about 344 °C with a weak shoulder in 284 °C could be attributed to the reduction of bulk NiO and surface free NiO species.[22,27] It is reported that the reduction of NiO and inter-diffusion of NiO and TiO_2 are a competitive process, thus, the peak in about 398 °C could be assigned to the reduction nickel titanate phase.[22] The broad feature between 500 °C and 800 °C could be attributed to titanium ions transported to the surface of nickel crystallites by a bulk diffusion mechanism.[22] V_2O_5/TiO_2 showed a strong reduction peak at 515 °C with a shoulder at 447 °C. TiO_2 support is known to be reduced at the temperature higher than 540 °C,[4] thus, the peaks at 447 °C and 515 °C could be ascribed to the reduction of bulk vanadia and highly dispersion vanadia on TiO_2 support.[4,28] The $V–Ni/TiO_2$ mainly showed two partially overlapped reduction peaks located at 295 °C and 356 °C, respectively. The low temperature peak could be related to the reduction of highly dispersed NiO-like surface species participate along with V^{5+}.[29] For the inter-diffusion of NiO and TiO_2 occurs during reduction, the presence of sub-surface nickel species formed by the diffusion of nickel ions into TiO_2 support is very probable.[22] The high temperature reduction peak could be assigned to the reduction nickel titanate phase as discussed above. As informed from Fig. 5, all reduction peaks corresponding to vanadia and nickel oxide on $V–Ni/TiO_2$ sample shifted to a low temperature range as nickel oxides introduced, indicating that the interaction of nickel species and vanadium species can improve the reducibility of oxygen species on the surface of this catalyst, which would be beneficial for the destruction of DCM and its intermediates, since the catalytic activities of all investigated samples are basically in line with their redox properties (shown in Fig. 1).

3.2.3 NH_3-TPD results. The acidic properties of catalyst were found to have significantly influence on the activity in CVOCs oxidation. The strength and amount of acidic sites were reflected in the desorption temperature and in the peak area of a
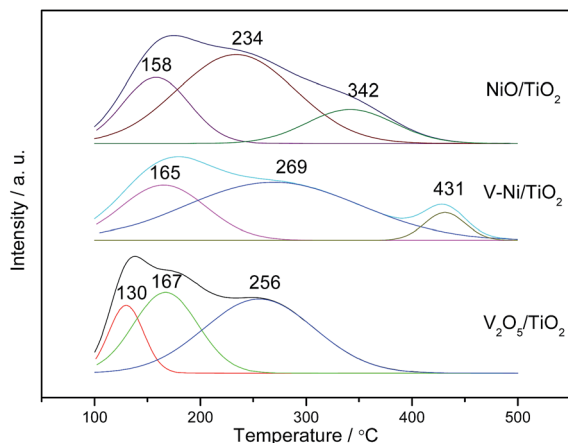
Fig. 6 NH_3-TPD profiles of investigated samples.

Fig. 8 Raman patterns after pyridine adsorption of as-prepared samples.

plot of temperature-programmed desorption of NH_3 (NH_3-TPD). The surface acidic natures of all investigated samples are shown in Fig. 6. In all cases, a wide desorption peak could be seen in the temperature range of 100–500 °C, which could be fitted into three peaks through deconvolution. The sites retaining NH_3 at temperature higher than 275 °C could be ascribed to strong acidic sites,[30] also the desorption peaks located at ~250 °C and ~150 °C indicate that the samples possess medium acidic sites and weak acidic sites,[31] respectively. As informed from Fig. 6, only weak and medium acidic sites presented on V_2O_5/TiO_2, however, all of weak, medium and strong acidic sites could be observed on NiO/TiO_2 and $V–Ni/TiO_2$ with different intensities. It is generally accepted that the medium and strong acidic sites are active sites in CVOCs oxidation. Compared with V_2O_5/TiO_2 and NiO/TiO_2, the medium and strong acidic sites over $V–Ni/TiO_2$ were much stronger, which be beneficial for the destruction of DCM.[32]

3.2.4 Raman spectroscopy results. Raman spectroscopy, known to be highly sensitive for detecting V=O bond vibration in vanadium oxides, was performed for the as-prepared samples. As shown in Fig. 7, the strong Raman absorption bands at 636, 514, and 394 cm^{-1} could be ascribed to E_g, A_{1g} + B_{1g}, and B_{1g} vibration modes in TiO_2 (anatase).[33,34] Generally,

the bulk vanadium at a low concentration resulting from V=O bond was prevalently located at around 1030 cm^{-1} in Raman spectra.[35] The V_2O_5/TiO_2 catalyst exhibited two weak absorption bands at 1030 and 993 cm^{-1}, which could be attributed to the vibrations of terminal V=O bond stretch and V_2O_5 microcrystalline,[36] respectively, the result is consistent with that of XRD patterns. For $V–Ni/TiO_2$ sample, the characteristic bands of V=O bond could not be observed, however, a band located at about 822 cm^{-1} could be attributed to the V–O stretching modes in $Ni_3V_2O_8$.[37,38] The formation of $Ni_3V_2O_8$ on $V–Ni/TiO_2$ is also consistent with the phase diagrams of $NiO–V_2O_5$ system.[39] Since this compound cannot be observed in the XRD pattern, probably it is presented in an amorphous form on the surface of $V–Ni/TiO_2$, or the particle sizes are too small to be identified by the conventional X-ray diffraction method. The coexistence of $Ni_3V_2O_8$ and NiO can also favor the specific surface area of $V–Ni/TiO_2$,[40] as shown in Table 1. Raman peaks located at about 473 cm^{-1} and 550 cm^{-1} are usually attributed to the Ni–O bond bending vibration and stretching vibration,[41,42] respectively; these peaks could not be clearly observed since they are overlapped with the strong vibration modes of TiO_2 (anatase).

The acidic natures of as-prepared samples are also investigated by Raman spectra after pyridine adsorption, and the results are shown in Fig. 8.

As can be seen, the $V–Ni/TiO_2$ sample showed two absorption bands at 991 and 1030 cm^{-1}, which could be attributed to the U_1 and U_{12} modes of ring-breathing vibrations (UCCN) of liquid pyridine,[43,44] corresponding to physically adsorbed pyridine. The strong absorption band at 1016 cm^{-1} in $V–Ni/TiO_2$ and NiO/TiO_2 samples, was due to the U_1 mode of ring-breathing vibration (UCCN), resulting from pyridine coordination to Lewis acidic sites.[44,45] The absorption band at 3077 cm^{-1} in $V–Ni/TiO_2$ sample could be ascribed to pyridine adsorbed on Lewis acidic sites overlapping with hydrogen bonded pyridine.[43]

4. Stability test of catalysts

The stability of catalysts in DCM combustion was investigated in a 100 h continuous test at 300 °C. As shown in Fig. 9, all
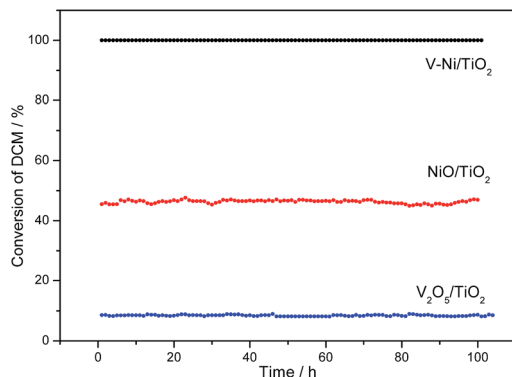

Fig. 7 Raman patterns of investigated samples.

Fig. 9 Stability test of catalysts in DCM conversion at 300 °C; gas composition: 1000 ppm DCM, 20.8% O_2, N_2 balance, GHSV = 15 000 mL g^{-1} h^{-1}.

samples showed good stabilities during long-term test. DCM conversion could be maintained above 99% over V–Ni/TiO$_2$ catalyst, no deactivation phenomenon could be observed. It is generally accepted that both the reducibility and acidic properties are responsible for the performance of transition metal oxide catalysts in CVOCs oxidation.[46] As informed from Fig. 6, the strength and the amount of medium and strong acidic sites on V–Ni/TiO$_2$ were more than those on V$_2$O$_5$/TiO$_2$, which would be beneficial for the destruction of DCM and the intermediates. However, the NiO/TiO$_2$ sample with comparative medium and strong acidic sites didn't show corresponding activity as V–Ni/TiO$_2$, this means the reducibility of catalyst may also play an important role in DCM oxidation. As shown in Fig. 5, the V–Ni/TiO$_2$ sample showed better reducibility than the NiO/TiO$_2$ and V$_2$O$_5$/TiO$_2$ samples, also the coexistence of Ni$_3$V$_2$O$_8$ and NiO (shown in Fig. 4 and 7, respectively) on the surface of V–Ni/TiO$_2$ also favoured the oxidative dehydrogenation ability of V–Ni/TiO$_2$,[40] thus, the V–Ni/TiO$_2$ showed good activity during long term exposure to DCM.

5. TEM of V–Ni/TiO$_2$ catalyst

For nickel-rich catalyst, the carbon deposit is very probable during the long-term running in DCM oxidation, thus, the morphology of fresh and used V–Ni/TiO$_2$ (after 100 h
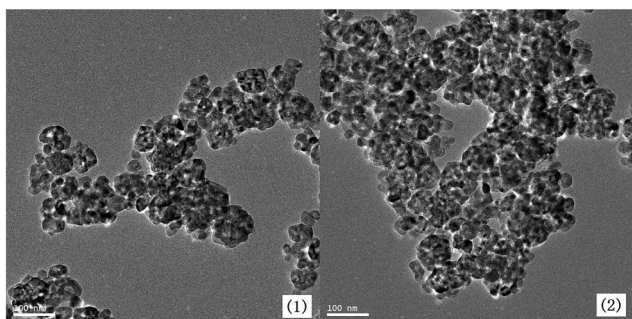

Fig. 10 TEM of fresh (1) and used ((2), after 100 h continuous test) of V–Ni/TiO$_2$.

Table 2 Some work made on total oxidation of DCM with transition metal oxide catalysts

Ref.	Catalyst(s) used	DCM content/ppm	GHSV	T_{90}/°C
15	4Ce1Cr	1000	15 000 h^{-1}	335
2	V$_2$O$_5$/Al$_2$O$_3$–TiO$_2$	500	32 000 h^{-1}	420
9	Ru/7%Ce–Al$_2$O$_3$	700	10 000 h^{-1}	260
48	CoCr$_2$O$_4$-4	3000	15 000 h^{-1}	257
49	CeZr	1000	71 m^3 kg^{-1} h^{-1}	467
46	VO$_x$/TiO$_2$-SG	1000	15 000 h^{-1}	313
This work	V–Ni/TiO$_2$	1000	15 000 mL g^{-1} h^{-1}	290

continuous test) were observed in TEM, as shown in Fig. 10. No significant differences could be observed between the fresh and aged samples, also no filamentous carbon could be observed on the surface of aged sample,[47] suggesting a high coke resistance ability of V–Ni/TiO$_2$ catalyst.

DCM catalytic combustion is a common model reaction in CVOCs oxidation. Based on transition metal oxide catalysts, our work is compared with those recently reported in literatures, and the results are listed in Table 2.

It should be mentioned that it is very difficult to compare the results of our work with those reported in the literatures, since the activity of the tested catalysts is significantly related to the operation conditions used. As listed in Table 2, the activity of V–Ni/TiO$_2$ sample is superior to most of catalysts listed, such as 4Ce1Cr, V$_2$O$_5$/Al$_2$O$_3$–TiO$_2$, CeZr mixed oxide and VO$_x$/TiO$_2$-SG, only inferior to that of Ru/7%Ce–Al$_2$O$_3$ and CoCr$_2$O$_4$-4.

6. Plausible mechanism for DCM decomposition over V–Ni/TiO$_2$ catalyst

It is reported by Gai et al.[50] that the presence of oxygen vacancies associated with the Lewis acidic centers of catalyst, DCM could be adsorbed on these oxygen vacancies in two ways through the relatively negative chlorine at a low temperature.[51] One is bridge–bounded DCM, in which DCM is adsorbed through the two chlorine atoms (1). The other is line–bounded DCM; in this case, DCM is adsorbed through a chlorine apex (2). The adsorbed DCM could be attacked by the adjacent nucleophilic [O] (O$^-$ and/or O^{2-}) species, the two chlorine atoms are substituted by
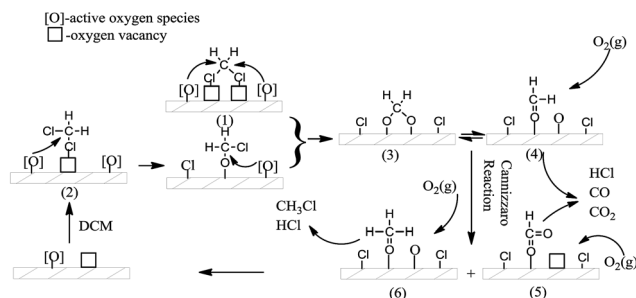

Fig. 11 A plausible mechanism for DCM combustion over V–Ni/TiO$_2$.

oxygen atoms analogous to S_N2 reaction, resulting the surface absorbed species (3) and formaldehyde species (4). The Cannizzaro reaction between (3) and (4) gives the adsorbed formate species (5) and methoxy species (6).[51] The mixture of vanadia and nickel oxide modified not only the redox properties of the system but also the acid–base characters of the oxygen species on V–Ni/TiO$_2$ catalyst,[40] as shown in Fig. 6 and 8, respectively; as well as the coexistence of NiO and Ni$_3$V$_2$O$_8$ on V–Ni/TiO$_2$ catalyst with p-type semiconductor nature promotes its oxidative dehydrogenation ability,[40] thus, the complete destruction of DCM and its intermediates could be attained at a lower temperature as compared with the other two mono-component catalysts. Based on the above discussions, a plausible reaction mechanism can be proposed for catalytic combustion of DCM over V–Ni/TiO$_2$ catalyst, as shown in Fig. 11.

7. Conclusions

V$_2$O$_5$ and/or NiO modified TiO$_2$ (anatase) catalysts were prepared by impregnation method and investigated in catalytic combustion of DCM. Both acidic and redox properties play important roles in deep oxidation of DCM. V–Ni/TiO$_2$ exhibits the best activity and stability for the model compound selected. The coexistence of NiO and Ni$_3$V$_2$O$_8$, good reducibility and oxidative dehydrogenation ability, as well as high intensity of medium and strong Lewis acidic sites and high coke resistance ability of the catalyst, are responsible for the destruction of DCM and its intermediates at a low-temperature range; therefore, the V–Ni/TiO$_2$ catalyst shows good stability during long term exposure to DCM.

Acknowledgements

Notes and references

1 I. Maupin, L. Pinard, J. Mijoin and P. Magnoux, *J. Catal.*, 2012, **291**, 104–109.

2 S. Pitkäaho, T. Nevanperä, L. Matejova, S. Ojala and R. L. Keiski, *Appl. Catal., B*, 2013, **138–139**, 33–42.

3 S. Pitkäaho, L. Matejova, S. Ojala, J. Gaalova and R. L. Keiski, *Appl. Catal., B*, 2012, **113–114**, 150–159.

4 M. Wu, K. C. Ung, Q. Dai and X. Wang, *Catal. Commun.*, 2012, **18**, 72–75.

5 Q. Huang, X. Xue and R. Zhou, *J. Mol. Catal. A: Chem.*, 2011, **344**, 74–82.

6 B. de Rivas, N. Guillén-Hurtado, R. López-Fonseca, F. Coloma-Pascual, A. García-García, J. I. Gutiérrez-Ortiz and A. Bueno-López, *Appl. Catal., B*, 2012, **121–122**, 162–170.

7 Q. Dai, S. Bai, Z. Wang, X. Wang and G. Lu, *Appl. Catal., B*, 2012, **126**, 64–75.

8 R. Ma, P. Hu, L. Jin, Y. Wang, J. Lu and M. Luo, *Catal. Today*, 2011, **175**, 598–602.

9 L. Ran, Z. Wang and X. Wang, *Appl. Catal., A*, 2014, **470**, 442–450.

10 R. López-Fonseca, J. I. Gutiérrez-Ortiz and J. R. González-Velasco, *Appl. Catal., A*, 2004, **271**, 39–46.

11 L. Intriago, E. Díaz, S. Ordóñez and A. Vega, *Microporous Mesoporous Mater.*, 2006, **91**, 161–169.

12 A. Aranzabal, M. Romero-Sáez, U. Elizundia, J. R. González-Velasco and J. A. González-Marcos, *J. Catal.*, 2012, **296**, 165–174.

13 A. Z. Abdullah, M. Z. A. Bakar and S. Bhatia, *J. Hazard. Mater.*, 2006, **129**, 39–49.

14 S. Ojala, S. Pitkaaho, T. Laitinen, N. N. Koivikko, R. Brahmi, J. Gaalova, L. Matejova, A. Kucherov, S. Paivarinta, C. Hirschmann, T. Nevanpera, M. Riihimaki, M. Pirila and R. L. Keiski, *Top. Catal.*, 2011, **54**, 1224–1256.

15 P. Yang, S. Yang, Z. Shi, Z. Meng and R. Zhou, *Appl. Catal., B*, 2015, **162**, 227–235.

16 G. Deo and I. E. Wachs, *J. Catal.*, 1994, **146**, 323–334.

17 G. Deo and I. E. Wachs, *J. Catal.*, 1994, **146**, 335–345.

18 Q. Dai, S. Bai, H. Li, W. Liu, X. Wang and G. Lu, *Appl. Catal., B*, 2015, **168–169**, 141–155.

19 R. W. van den Brink, P. Mulder, R. Louw, G. Sinquin, C. Petit and J. Hindermann, *J. Catal.*, 1998, **180**, 153–160.

20 L. Pinard, J. Mijoin, P. Ayrault, C. Canaff and P. Magnoux, *Appl. Catal., B*, 2004, **51**, 1–8.

21 X. Zhang, J. Liu, Y. Jing and Y. Xie, *Appl. Catal., A*, 2003, **240**, 143–150.

22 B. Aristizábal, C. A. González, I. Barrio, M. Montes and C. Montes de Correa, *J. Mol. Catal. A: Chem.*, 2004, **222**, 189–198.

23 Y. Liu, L. Fu and Y. Tang, *Fenzi Cuihua*, 1989, **3**, 173–180.

24 Q. Dai, X. Wang and G. Lu, *Appl. Catal., B*, 2008, **81**, 192–202.

25 C. Yang, W. Wang, Z. Shan and F. Huang, *J. Solid State Chem.*, 2009, **182**, 807–812.

26 L. Li, B. Cheng, Y. Wang and J. Yu, *J. Colloid Interface Sci.*, 2015, **449**, 115–121.

27 B. Agula, Q. Deng, M. Jia, Y. Liu, B. Zhaorigetu and Z. Yuan, *React. Kinet., Mech. Catal.*, 2011, **103**, 101–112.

28 A. Nie, H. Yang, Q. Li, X. Fan, F. Qiu and X. Zhang, *Ind. Eng. Chem. Res.*, 2011, **50**, 9944–9948.

29 V. P. Vislovskiy, N. T. Shamilov, A. M. Sardarly, R. M. Talyshinskii, V. Y. Bychkov, P. Ruiz, V. Cortes Corberan, Z. Schay and Z. Koppany, *Appl. Catal., A*, 2003, **250**, 143–150.

30 B. de Rivas, R. Lopez-Fonseca, M. A. Gutierrez-Ortiz and J. I. Gutierrez-Ortiz, *Appl. Catal., B*, 2011, **104**, 373–381.

31 L. Matějová, P. Topka, L. Kaluža, S. Pitkäaho, S. Ojala, J. Gaálová and R. L. Keiski, *Appl. Catal., B*, 2013, **142–143**, 54–64.

32 P. Yang, X. Xue, Z. Meng and R. Zhou, *Chem. Eng. J.*, 2013, **234**, 203–210.

33 S. Yamauchi and Y. Imai, *Cryst. Struct. Theory Appl.*, 2013, **2**, 1–7.

34 P. C. Ricci, C. M. Carbonaro, L. Stagi, M. Salis, A. Casu, S. Enzo and F. Delogu, *J. Phys. Chem. C*, 2013, **117**, 7850–7857.

35 S. Youn, S. Jeong and D. H. Kim, *Catal. Today*, 2014, **232**, 185–191.

36 I. Giakoumelou, C. Fountzoula, C. Kordulis and S. Boghosian, *J. Catal.*, 2006, **239**, 1–12.

37 A. Klisińska, S. Loridant, B. Grzybowska, J. Stoch and I. Gressel, *Appl. Catal., A*, 2006, **309**, 17–27.

38 Y. Seo, S. Kim, J. Ahn and I. Jeong, *J. Korean Phys. Soc.*, 2013, **62**, 116–120.

39 V. L. Kozhevnikov, S. M. Chesnitskii and V. V. Strelkov, *Term. Anal. Fazovye Ravnovesiya*, 1987, 96–99.

40 Z. Bao, W. Li, R. Kieffer and H. Xu, *React. Kinet. Catal. Lett.*, 2002, **75**, 275–287.

41 G. Cai, J. Tu, D. Zhou, L. Li, J. Zhang, X. Wang and C. Gu, *J. Phys. Chem. C*, 2014, **118**, 6690–6696.

42 M. A. Vuurman, D. J. Stufkens, A. Oskam, G. Deo and I. E. Wachs, *J. Chem. Soc., Faraday Trans.*, 1996, **92**, 3259–3265.

43 H. Yamada and Y. Yamamoto, *J. Chem. Soc., Faraday Trans. 1*, 1979, **75**, 1215–1221.

44 P. Yuan, D. Q. Wu, H. P. He and Z. Y. Lin, *Appl. Surf. Sci.*, 2004, **227**, 30–39.

45 G. L. Schrader and C. P. Cheng, *J. Phys. Chem.*, 1983, **87**, 3675–3681.

46 M. Wu, K. C. Ung, Q. G. Dai and X. Y. Wang, *Catal. Commun.*, 2012, **18**, 72–75.

47 Q. Liu, F. Gu, X. Lu, Y. Liu, H. Li, Z. Zhong, G. Xu and F. Su, *Appl. Catal., A*, 2014, **488**, 37–47.

48 Y. Wang, A. Jia, M. Luo and J. Lu, *Appl. Catal., B*, 2014, **165**, 477–486.

49 L. Matejova, P. Topka, L. Kaluza, S. Pitkaaho, S. Ojala, J. Gaalova and R. L. Keiski, *Appl. Catal., B*, 2013, **142**, 54–64.

50 P. L. Gai and K. Kourtakis, *Science*, 1995, **267**, 661–663.

51 J. Haber, T. Machej, M. Derewiński, R. Janik, J. Kryściak, H. Sadowska and J. Janas, *Catal. Today*, 1999, **54**, 47–55.